Excitonic effects on radial breathing mode intensity of single wall carbon nanotubes

Kentaro Sato[a,*], Riichiro Saito[b], Ahmad R.T. Nugraha[b], Shigeo Maruyama[a]

[a] *Department of Mechanical Engineering, School of Engineering, The University of Tokyo, Japan*
[b] *Department of Physics, Tohoku University, Sendai, 980-8578, Japan*

Abstract

We develop exciton-photon and exciton-phonon interaction matrix elements for single wall carbon nanotubes within extended tight binding method. The exciton-photon matrix elements using the extended tight binding wave function have a large chirality dependence compared with the previous calculation by simple tight binding method. Using the exciton-photon and exciton-phonon matrix elements presented here, we calculate resonance Raman intensity for radial breathing mode as a function of diameter and chiral angle. Excitonic effect of resonance Raman intensities for the radial breathing mode is enhanced by the curvature and trigonal warping effects.

1. Introduction

Resonance Raman spectroscopy has been well developed for optical characterization of single wall carbon nanotubes (SWNTs) [1–3]. Since a photo-excited electron and hole are strongly bound by the Coulomb interaction in the quasi-one-dimensional system, excitonic effects of SWNTs appear even at the room temperature in the Raman spectra. The optical transition energies are denoted by E_{ii}, which are transitions between the i-th conduction and the i-th valence energy subbands, or bright exciton energies [4–9]. Especially, Raman shift and intensity of radial breathing mode (RBM) of a SWNT depend on diameter d_t, and chirality (n, m), which are relevant to the excitonic effects of a SWNT [9–13]. Thus calculation of RBM intensities as a function of

*Corresponding author
Email address: kentaro@photon.t.u-tokyo.ac.jp (Kentaro Sato)

(n, m) are frequently used for evaluating the population of (n, m) SWNTs in the sample [14, 15].

Experimental and theoretical results have demonstrated that the excitonic effects contribute strongly to the optical characterization of SWNTs [7, 16, 17]. Jiang *et al*. developed and calculated the exciton-photon, exciton-phonon matrix elements, and resonance Raman intensities by the exciton picture within simple (the nearest neighbor) tight binding scheme (STB) for only π electrons [9]. Since π orbitals are mixed with σ orbitals by the curvature effects of a SWNT [18], we have to use the extended tight binding (ETB) wave function for obtaining more accurate exciton-photon and exciton-phonon matrix elements. It is noted that Jiang *et al*. used ETB wave function for calculating exciton E_{ii} energies [8], but that they adapted STB wave function for calculating exciton-photon and exciton-phonon matrix elements for simplicity. Recently, Pesce *et al*. have reported RBM Raman intensity as a function of diameter and chiral angle [14], In order to compare with the experimental results, we improve the exciton calculations to the ETB exciton-photon and exciton-phonon matrix elements, which is the main message of this paper.

In Sec. II, we show an outline of the calculation method for exciton-photon and exciton-phonon matrix elements, and resonance Raman intensity within ETB scheme. In Sec. III we show calculated results of the exciton-photon and exciton-phonon matrix elements, and resonance Raman intensity for RBM as a function $d_{\rm t}$ and chiral angle θ. We also compare our calculation results based on ETB with the previous calculation results [9] based on STB and the recent experimental results [14]. Finally, summary of the present work is given in Sec. IV.

2. Method

The exciton energy and exciton wave function coefficients are calculated by solving the Bethe-Salpeter equation [7–9, 16]. In this paper, we calculate exciton energy, exciton wave function, exciton-photon and exciton-phonon matrix elements based on ETB. In the calculation, however, we consider the Coulomb interaction only for π electrons and we adopt the random phase approximation for a polarization function of the

π electrons [8]. To describe the Coulomb interaction of π electrons, we use the Ohno potential which is widely used for one-dimensional conductors [19]. The Coulomb interaction for σ electrons and the surrounding materials is expressed by a static dielectric constant κ [12, 20, 21]. Hereafter we use the dielectric constant $\kappa = 2$ in the calculation which reproduces the experimental values of the Raman E_{ii} or PL E_{ii} for SWNT bundle samples within a limited range of $d_{\rm t}$ and E_{ii} [8]. Since dielectric constant depends on nanotube diameter and E_{ii} [12, 21], we should consider the effects of different surrounding materials which is knows as environmental effect, which will be given elsewhere [20].

The exciton-photon matrix elements between an excited state $|\Psi_0^n\rangle$ and the ground state $|0\rangle$ in the dipole approximation are expressed as [9]

$$M_{\rm ex-op} = \langle \Psi_0^n | H_{\rm el-op} | 0 \rangle, \tag{1}$$

where $H_{\rm el-op}$ is the electron-photon Hamiltonian. Due to the selection rule for the wave vector in the parallel polarization, we can write $H_{\rm el-op}$ as [9]

$$H_{\rm el-op} = \sum_{\boldsymbol{k}} D_{\boldsymbol{k}} c_{\boldsymbol{k}c}^\dagger c_{\boldsymbol{k}v} (a + a^\dagger), \tag{2}$$

where $D_{\boldsymbol{k}}$ is the z component of the dipole vector between the initial and final states [22], $c_{\boldsymbol{k}c}^\dagger$ ($c_{\boldsymbol{k}v}$) is the electron creation (annihilation) operator in the conduction (valence) band, and $a^\dagger$ (a) is the photon creation (annihilation) operator. The exciton wave function $|\Psi_{\boldsymbol{q}}^n\rangle$ with a center-of-mass momentum $\boldsymbol{q}$ is expressed as

$$|\Psi_{\boldsymbol{q}}^n\rangle = \sum_{\boldsymbol{k}} Z_{\boldsymbol{k}c,(\boldsymbol{k}-\boldsymbol{q})v}^n c_{\boldsymbol{k}c}^\dagger c_{(\boldsymbol{k}-\boldsymbol{q})v} |0\rangle, \tag{3}$$

where $Z_{\boldsymbol{k}c,(\boldsymbol{k}-\boldsymbol{q})v}^n$ is the eigen vector of the n-th ($n = 1, 2, \dots$) state of the Bethe-Salpeter equation. Instead of summation over all cutting lines (one-dimensional Brillouin zone (BZ) plotted in two-dimensional BZ [23, 24]) of $\boldsymbol{k}$ states, we can use a single cutting line of $\boldsymbol{k}$ state for the summation [9]. From Eq.(1)-(3), the exciton-photon matrix elements between an excited state and the ground state are written as

$$M_{\rm ex-op} = \sum_{\boldsymbol{k}} D_{\boldsymbol{k}} Z_{\boldsymbol{k}c,\boldsymbol{k}v}^{n*}. \tag{4}$$

$Z^{n*}_{\boldsymbol{k}c,\boldsymbol{k}v}$ and $D_{\boldsymbol{k}}$ are calculated by solving Bethe-Salpeter equation within ETB scheme [8, 18], in which we use ETB wave function which takes account of curvature and trigonal warping effects in spite of STB wave function [18]. From the symmetry of the exciton wave function under a C_2 rotation around an axis perpendicular to nanotube axis, the exciton of a SWNT is classified as either optically active (bright exciton) or optically inactive (dark exciton) [25, 26]. Hereafter we only consider bright exciton states.

The exciton-phonon matrix elements $M_{\mathrm{ex-ph}}$ between the initial state $|\Psi^{n_1}_{\boldsymbol{q}_1}\rangle$ and a final state $|\Psi^{n_2}_{\boldsymbol{q}_2}\rangle$ are expressed by

$$M_{\mathrm{ex-ph}} = \langle\Psi^{n_2}_{\boldsymbol{q}_2}|H_{\mathrm{el-ph}}|\Psi^{n_1}_{\boldsymbol{q}_1}\rangle, \tag{5}$$

where $H_{\mathrm{el-ph}}$ is the Hamiltonian for the electron-phonon coupling for the ν-th phonon mode and a phonon wave vector $\boldsymbol{q} = \boldsymbol{q}_1 - \boldsymbol{q}_2$ [27],

$$\begin{aligned} H_{\mathrm{el-ph}} = \sum_{\boldsymbol{k}q\nu} \Big[& M^{\nu}_{\boldsymbol{k},\boldsymbol{k}+q}(c) c^{\dagger}_{(\boldsymbol{k}+\boldsymbol{q})c} c_{\boldsymbol{k}c} \\ & - M^{\nu}_{\boldsymbol{k},\boldsymbol{k}+q}(v) c^{\dagger}_{(\boldsymbol{k}+\boldsymbol{q})v} c_{\boldsymbol{k}v} \Big] (b_{\boldsymbol{q}\nu} + b^{\dagger}_{\boldsymbol{q}\nu}), \end{aligned} \tag{6}$$

where $M(c)$ ($M(v)$) is the electron-phonon matrix element for the conduction (valence) band. $b^{\dagger}_{\boldsymbol{q}\nu}$ ($b_{\boldsymbol{q}\nu}$) is a phonon creation (annihilation) operator for the ν-th phonon mode $\boldsymbol{q}$. Finally, we get the exciton-phonon matrix elements as follows

$$\begin{aligned} M_{\mathrm{ex-ph}} =& \langle\Psi^{n_2}_{\boldsymbol{q}_2}|H_{\mathrm{el-op}}|\Psi^{n_1}_{\boldsymbol{q}_1}\rangle \\ =& \sum_{\boldsymbol{k}} \Big[M^{\nu}_{\boldsymbol{k},\boldsymbol{k}+q}(c) Z^{n_2 *}_{(\boldsymbol{k}+\boldsymbol{q})c,(\boldsymbol{k}-\boldsymbol{q}_1)v} Z^{n_1}_{\boldsymbol{k}c,(\boldsymbol{k}-\boldsymbol{q}_1)v} \\ & - M^{\nu}_{\boldsymbol{k},\boldsymbol{k}+q}(v) Z^{n_2 *}_{(\boldsymbol{k}+\boldsymbol{q}_2)c,\boldsymbol{k}v} Z^{n_1}_{(\boldsymbol{k}+\boldsymbol{q}_2)c,(\boldsymbol{k}+\boldsymbol{q})v} \Big]. \end{aligned} \tag{7}$$

All these calculations are treated within ETB scheme [27]. Using the exciton-photon and exciton-phonon matrix elements, resonance Raman intensity is calculated by

$$I_{\mathrm{ex}} \propto \left| \sum_{a} \frac{M_{\mathrm{ex-op}}(b) M_{\mathrm{ex-ph}}(a \to b) M_{\mathrm{ex-op}}(a)}{(E - E_a + i\gamma)(E - E_a - E_{\mathrm{ph}} + i\gamma)} \right|^2, \tag{8}$$

where γ is a broadening factor, E, E_a, and E_{ph} are energy of the excited light, exciton transition energy, and phonon energy, respectively [9]. In this paper we use a static

constant $\gamma = 0.06$ eV [3, 27], though Pesce *et al*. consider diameter and chiral angle dependence of γ [14]. In order to calculate diameter and chiral angle dependence of γ, we need to consider exciton-phonon interaction of not only for intravalley scattering but also intervalley scattering [30], which will be also a future work. In Eq.(8) we assume that the wave function of the virtual state $|b\rangle$ is approximated by that of the real state $|a\rangle$ [9]. We will only consider only the first-order resonance Raman process and the Stokes Raman (phonon emission) process.

3. Results and discussions

Figure 1 shows exciton-photon matrix elements of SWNTs for E_{22}^{S} and E_{11}^{M} as a function of diameter. Here the matrix elements are normalized by $N^{-1/2}$ (where N is the number of graphite unit cell in a SWNT [23]) for a diameter from 0.6 to 1.6 nm. Figure 1 (a) ((c)) is E_{22}^{S} (E_{11}^{M}) $M_{\mathrm{ex-op}}$ within ETB. For comparison we show E_{22}^{S} (E_{11}^{M}) $M_{\mathrm{ex-op}}$ within STB [9] in Fig. 1 (b) ((d)). The exciton-photon matrix elements within STB show d_{t}^{-1} dependence and no chirality dependence [9]. However, the exciton-photon matrix elements within ETB have a weak chirality dependence because of the trigonal warping effects [28]. The chiral angle dependence for type II ($\mathrm{mod}(2n+m, 3) = 2$) [29] semiconducting SWNTs (s-SWNTs) is larger than that for type I ($\mathrm{mod}(2n + m, 3) = 1$) s-SWNTs. Thus optical absorption intensity of SWNTs is expected to have d_{t}^{-2} dependence and chirality dependence. The exciton-photon matrix elements within ETB are larger than those within STB because the ETB exciton wave functions are more localized from STB exciton wave functions for all diameters.

Figure 2 shows exciton-phonon matrix elements $M_{\mathrm{ex-ph}}$ at k_{ii} which gives the maximum Z_k of RBM for E_{22}^{S} and E_{11}^{M} as a function of diameter. We calculate the exciton-phonon matrix elements using Eq.(7) within a diameter range of $0.6 < d_{\mathrm{t}} < 1.6$ nm. Figure 2 (a) ((c)) is E_{22}^{S} (E_{11}^{M}) $M_{\mathrm{ex-op}}$ for RBM within ETB. For comparison we show E_{22}^{S} (E_{11}^{M}) $M_{\mathrm{ex-op}}$ for RBM within STB [9] in Fig. 2 (b) ((d)). The exciton-phonon matrix elements of RBM by ETB are almost the same as that by STB, since exciton wave function Z_k does not change much between STB and ETB [9]. Thus we expect that difference between ETB and STB exciton-phonon matrix elements are not significant.

The $2n + m$ = constant family pattern for (n, m) SWNT is shown by solid curves with family numbers $(2n + m)$ in Fig. 2. As seen in Fig. 2, the matrix elements of armchair nanotubes are almost zero. Exciton-phonon matrix elements have strong chirality dependence compared with exciton-photon matrix elements. Thus chirality dependence on resonance Raman intensity for RBM depends mainly on exciton-phonon matrix elements.

Figure 3 shows a relation between the exciton wave function coefficients and the electron-phonon matrix elements as a function of 1D k on the cutting line (1D Brillouin zone) [24]. For $(10, 0)$ zigzag nanotube (Fig. 3(a)) the electron-phonon matrix elements have the same sign in the region that exciton wave function coefficients have a value. On the other hand, near armchair nanotubes, (e.g. $(7, 6)$ nanotube in Fig. 3(b)) the sign of the electron-phonon matrix elements has a node at the k point. Since the exciton-phonon matrix element is given by the integration of the exciton coefficient multiplied by the electron-phonon matrix element, exciton-phonon matrix element decreases with increasing the chiral angle.

Using $M_{\mathrm{ex-op}}$ and $M_{\mathrm{ex-ph}}$, we calculate resonance Raman intensities for RBM by Eq.(8). Figure 4 shows the diameter dependence of E_{22}^{S} and E_{11}^{M} resonance Raman intensity of RBM for SWNTs. Figure 4 (a) ((c)) is E_{22}^{S} (E_{11}^{M}) I_{ex} for RBM within ETB. For comparison we show E_{22}^{S} (E_{11}^{M}) I_{ex} for RBM within STB [9] in Fig. 1 (b) ((d)). From chirality dependence on the exciton-photon and the exciton-phonon matrix elements within ETB, chirality dependence on the resonance Raman intensity with ETB is enhanced. Equation (8) shows that the Raman intensity is proportional to $|M_{\mathrm{ex-op}}^4 M_{\mathrm{ex-ph}}|^2$. Since the effects of the many neighbors are included into the ETB calculation, the excitonic effects of the matrix elements are enhanced significantly. The Raman intensity of near zigzag nanotubes is one-order of magnitude stronger than that of near armchair nanotubes. Thus we expect to observe a stronger RBM intensity from zigzag nanotubes in experiments if homogeneous population if assumed for (n, m) SWNTs.

Pesce *et al*. reported a diameter and chirality dependence of RBM intensity from resonance Raman scattering and high resolution transmission electron microscopy measurements for 395 different SWNTs [14]. To fit the experimental RBM intensity to an empirical function of d_{t} and θ, they assume that the numerator $M = |M_{\mathrm{ex-op}}(a) M_{\mathrm{ex-ph}}(a \rightarrow$

$b)M_{\mathrm{ex-op}}(b)|^2$ and the broadening factor γ in Eq.(8) have a diameter and chirality dependence. Here we consider a similar fitting function for the numerator in Eq.(8) to compare our calculated RBM intensity with experimental RBM intensity.

$$M = \frac{A}{d_t} + \frac{B\cos(3\theta)}{d_t} + \frac{C}{d_t^2} + \frac{D\cos(3\theta)}{d_t^2} + \frac{E\cos^2(3\theta)}{d_t^2}. \tag{9}$$

θ is chiral angle, and A, B, C, D, E are fitting parameters. In table 1, we list the fitted values of A-E for Fig. 5 with the correlation coefficient R^2. We use Eq.(9) for numerator of Eq.(8) and fit the function to our calculated results. Figure 5 shows our calculated RBM intensity (solid circles) and fitted function (open circles) by using Eq.(9) which works sufficiently. Symbols are connected by $2n + m$ = constant family line. The inset of Fig. 5 is the difference between our calculated RBM intensity and the fitted function. The diameter and chirality dependence of the calculated RBM intensity is similar to that of Pesce *et al*. However, the RBM intensity of type I s-SWNTs reported by Pesce *et al*. is much larger than those for type II s-SWNTs or metallic nanotubes. In order to make consistency with the experiments, the population of type I s-SWNTs could be much larger than type II s-SWNTs. However, we don't have any special reason why we get a large population for type I s-SWNTs up to now. Moreover the calculated RBM intensity for (near) zigzag nanotubes of semiconducting type II deviates slightly from the fitting function which is due to a relatively small exciton-photon matrix element. It is the reason why R^2 values becomes relatively small for type II s-SWNTs. The exciton-photon matrix elements is the sum of the product of exciton wave function coefficient and dipole vector. Since the trigonal warping effects of the dipole vector for zigzag nanotubes become strong for type II s-SWNTs [28], the exciton-photon matrix elements becomes small especially for zigzag-SWNTs. In order to take into account this effect, we need to consider the chiral angle dependence of γ, which we don't consider in this paper.

The experimental γ values (the supplement data of Ref. [14]) show that γ value is a decreasing function of d_{t} and that the values are smaller than 0.06 eV for diameter larger than 1 nm. The calculated Raman intensity decreases with increasing d_{t} and θ, which is consistent with the experiment. In this comparison, we need to check the experimental results in order to carefully estimate the matrix elements over a wide

range of d_t, θ, and E_{ii}. We should consider population of (n, m) [31] and other exciton effect of environmental effect [20, 32], which we should wait for further experimental works for one nanotube measurement.

4. Summary

In conclusion, we have developed exciton-photon and exciton-phonon matrix elements based on the ETB scheme. Exciton-phonon matrix elements based on ETB is almost the same as that of STB. On the other hand exciton-photon matrix elements based on ETB has a weak chirality dependence. Moreover we have calculated E_{22}^{S} and E_{11}^{M} resonance Raman intensity for RBM by using ETB scheme in exciton picture. The chirality dependence of RBM intensity shows that zigzag (and smaller d_t) nanotube gives much larger RBM intensity than near armchair (and larger d_t) nanotube.

5. Acknowledgments

K.S. is supported by a JSPS research grant (No. 20-4594). R.S. acknowledges Professor A. Jorio, Mr. P.B.C. Pesce, and Professor M.S. Dresselhaus for variable discussion and support from MEXT Grants (No. 20241023). S.M. acknowledges part of this work was financially supported by Grants-in-Aid for Scientific Research (19054003 and 22246023) from the Japan Society for the Promotion of Science, SCOPE (051403009) from the Ministry of Internal Affairs and Communications, and "Development of Nanoelectronic Device Technology" of NEDO.

References

[1] M. S. Dresselhaus, G. Dresselhaus, R. Saito, and A. Jorio, Phys. Rep. 409 (2005) 47.

[2] C. Fantini, A. Jorio, M. Souza, M. S. Strano, M. S. Dresselhaus, and M. A. Pimenta, Phys. Rev. Lett. 93 (2004) 147406.

[3] A. Jorio, C. Fantini, M. A. Pimenta, R. B. Capaz, Ge. G. Samsonidze, G. Dresselhaus, M. S. Dresselhaus, J. Jiang, N. Kobayashi, A. Grüneis, and R. Saito, Phys. Rev. B 71 (2005) 075401.

[4] F. Wang, G. Dukovic, L. E. Brus, and T. F. Heinz, Science 308 (2005) 838.

[5] C. D. Spataru, S. Ismail-Beigi, L. X. Benedict, and S. G. Louie, Phys. Rev. Lett. 92 (2004) 077402.

[6] J. Maultzsch, R. Pomraenke, S. Reich, E. Chang, D. Prezzi, A. Ruini, E. Molinari, M. S. Strano, C. Thomsen, and C. Lienau, Phys. Rev. B 72 (2005) 241402.

[7] T. Ando, J. Phys. Soc. Jpn. 66 (1997) 1066.

[8] J. Jiang, R. Saito, Ge. G. Samsonidze, A. Jorio, S. G. Chou, G. Dresselhaus, and M. S. Dresselhaus, Phys. Rev. B 75 (2007) 035407.

[9] J. Jiang, R. Saito, K. Sato, J. S. Park, Ge. G. Samsonidze, A. Jorio, G. Dresselhaus, and M. S. Dresselhaus, Phys. Rev. B 75 (2007) 035405.

[10] P. T. Araujo, S. K. Doorn, S. Kilina, S. Tretiak, E. Einarsson, S. Maruyama, H. Chacham, M. A. Pimenta, and A. Jorio, Phys. Rev. Lett. 98 (2007) 067401.

[11] P. T. Araujo, I. O. Maciel, P. B. C. Pesce, M. A. Pimenta, S. K. Doorn, H. Qian, A. Hartschuh, M. Steiner, L. Grigorian, K. Hata, and A. Jorio, Phys. Rev. B 77 (2008) 241403.

[12] P. T. Araujo, A. Jorio, M. S. Dresselhaus, K. Sato, and R. Saito, Phys. Rev. Lett. 103 (2009) 146802.

[13] T. Michel, M. Paillet, J. C. Meyer, V. N. Popov, L. Henrard, and J.-L. Sauvajol, Phys. Rev. B 75 (2007) 155432.

[14] P. B. C. Pesce, P. T. Araujo, P. Nikolaev, S. K. Doorn, K. Hata, R. Saito, M. S. Dresselhaus, and A. Jorio, Appl. Phys. Lett. 96 (2010) 051910.

[15] E. H. Hároz, W. D. Rice, B. Y. Lu, S. Ghosh, R. H. Hauge, R. B. Weisman, S. K. Doorn, J. Kono, ACS Nano 4 (2010) 1955.

[16] T. Ando, J. Phys. Soc. Jpn. 73 (2004) 3351.

[17] T. Ando, J. Phys. Soc. Jpn. 75 (2006) 024707.

[18] Ge. G. Samsonidze, R. Saito, N. Kobayashi, A. Grüneis, J. Jiang, A. Jorio, S. G. Chou, G. Dresselhaus, and M. S. Dresselhaus, Appl. Phys. Lett. 85 (2004) 5703.

[19] K. Ohno, Theor. Chim. Acta 2 (1964) 219.

[20] A. R. T. Nugraha, R. Saito, K. Sato, P. T. Araujo, A. Jorio, and M. S. Dresselhaus, unpublished.

[21] Y. Miyauchi, R. Saito, K. Sato, Y. Ohno, S. Iwasaki, T. Mizutani, J. Jiang, and S. Maruyama, Chem. Phys. Lett. 442 (2007) 394.

[22] A. Grüneis, R. Saito, Ge. G. Samsonidze, T. Kimura, M. A. Pimenta, A. Jorio, A. G. Souza Filho, G. Dresselhaus, and M. S. Dresselhaus, Phys. Rev. B 67 (2003) 165402.

[23] R. Saito, G. Dresselhaus, and M. S. Dresselhaus, Physical Properties of Carbon Nanotubes, Imperial College Press, London, 1998.

[24] Ge. G. Samsonidze, R. Saito, A. Jorio, M. A. Pimenta, A. G. Souza Filho, A. Grüneis, G. Dresselhaus, and M. S. Dresselhaus, J. Nanosci. Nanotechnol. 3 (2003) 431.

[25] E. B. Barros, R. B. Capaz, A. Jorio, Ge. G. Samsonidze, A. G.Souza Filho, S. Ismail-Beigi, C. D. Spataru, S. G. Louie, G. Dresselhaus, and M. S. Dresselhaus, Phys. Rev. B 73 (2006) 241406(R).

[26] E. B. Barros, A. Jorio, Ge. G. Samsonidze, R. B. Capaz, A. G.Souza Filho, J. Mendez Filho, G. Dresselhaus, and M. S. Dresselhaus, Phys. Rep. 431 (2006) 261.

[27] J. Jiang, R. Saito, Ge. G. Samsonidze, S. G. Chou, A. Jorio, G. Dresselhaus, and M. S. Dresselhaus, Phys. Rev. B 72 (2005) 235408.

[28] R. Saito, G. Dresselhaus, and M. S. Dresselhaus, Phys. Rev. B 61 (200) 2981.

[29] R. Saito, K. Sato, Y. Oyama, J. Jiang, Ge. G. Samsonidze, G. Dresselhaus, M. S. Dresselhaus, Phys. Rev. B 72 (2005) 153413.

[30] J. Jiang, R. Saito, A. Grüneis, S. G. Chou, Ge. G. Samsonidze, A. Jorio, G. Dresselhaus, and M. S. Dresselhaus, Phys. Rev. B 71 (2005) 045417.

[31] A. Jorio, C. Fantini, M. A. Pimenta, D. A. Heller, M. S. Strano, M. S. Dresselhaus, Y. Oyama, J. Jiang, R. Saito, Appl. Phys. Lett. 88 (2006) 023109.

[32] T. Ando, J. Phys. Soc. Jpn. 79 (2010) 024706.

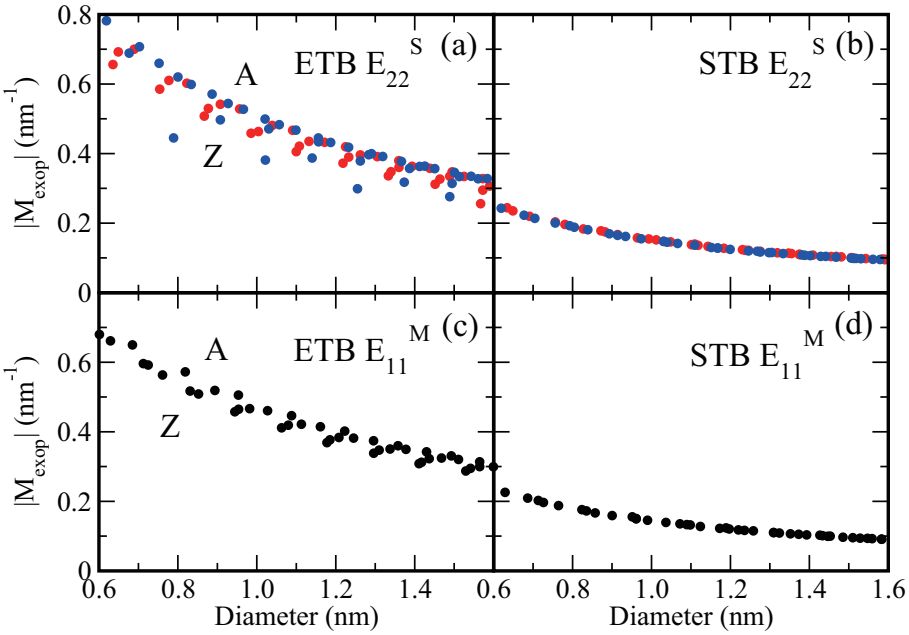

Figure 1: The diameter dependence on the exciton-photon matrix elements of SWNTs. (a) ((b)) is E_{22}^{S} $M_{\mathrm{ex-op}}$ within ETB (STB [9]). Here red (blue) circles are semiconducting type I (II) nanotubes. (c) ((d)) is E_{11}^{M} $M_{\mathrm{ex-op}}$ within ETB (STB [9]). Z (A) denotes chiral angle close to zigzag (armchair) nanotube.

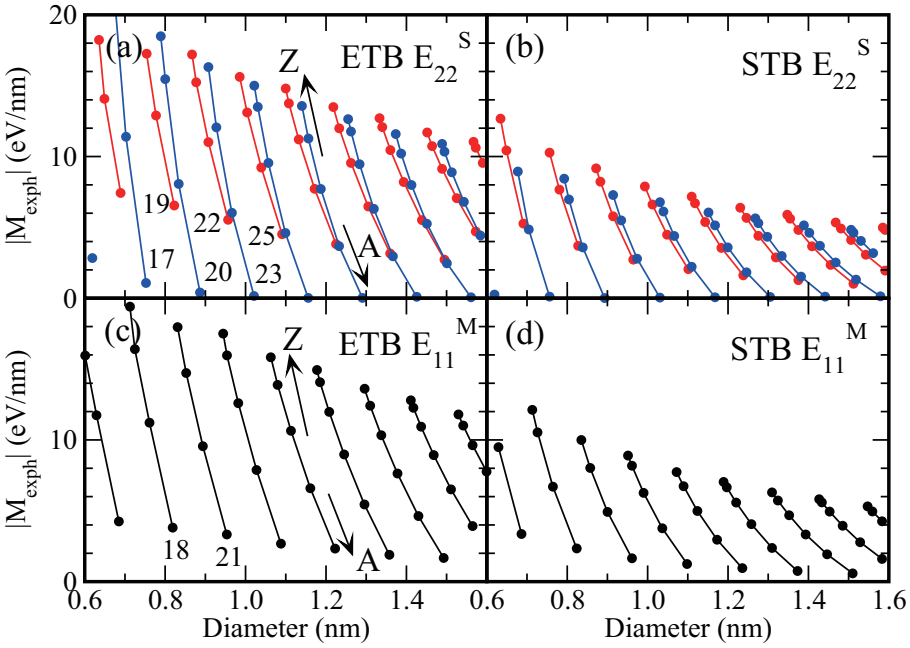

Figure 2: The diameter dependence of the exciton-phonon matrix elements for RBM of SWNTs. (a) ((b)) is $E_{22}^{\mathrm{S}}\, M_{\mathrm{ex-ph}}$ for RBM within ETB (STB [9]). Here red (blue) circles are semiconducting type I (II) nanotubes. (c) ((d)) is $E_{11}^{\mathrm{M}}\, M_{\mathrm{ex-ph}}$ for RBM within ETB (STB [9]). The family numbers $2n+m$ = constant are connected by the line. Z (A) denotes chiral angles close to zigzag (armchair) nanotube.

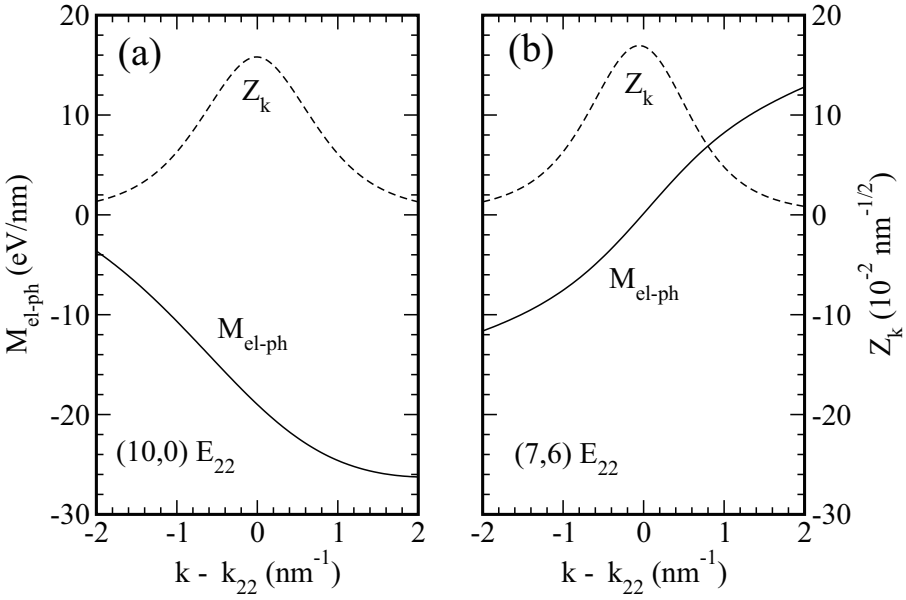

Figure 3: The electron-phonon matrix elements (solid line) and the absolute value of the E_{22} exciton wave function coefficients (dashed line) for (a) $(10, 0)$ nanotube (b) $(7, 6)$ nanotube.

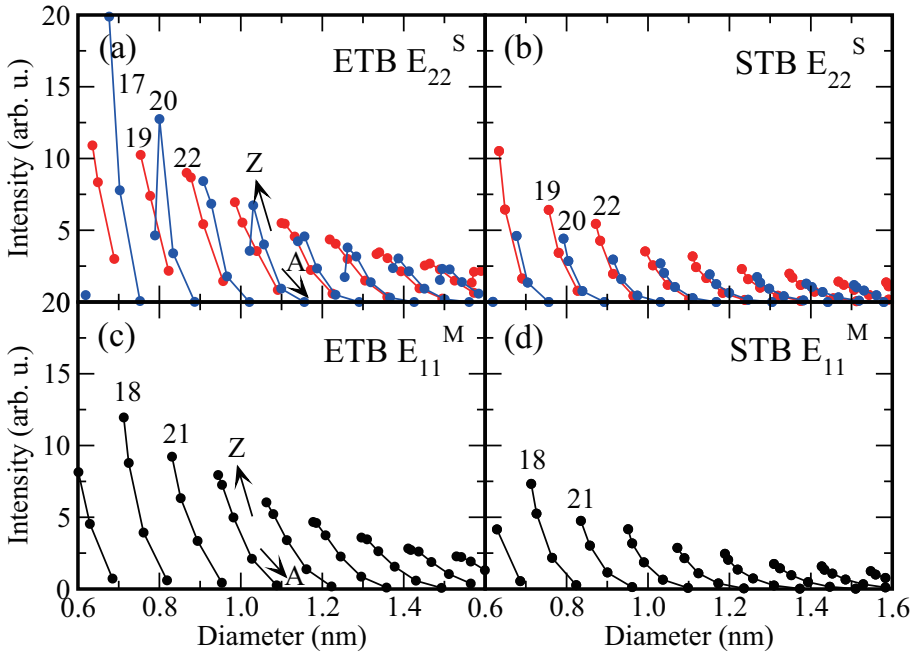

Figure 4: The diameter dependence of the resonance Raman intensity for RBM of SWNTs (intensity on log scale). (a) ((b)) is $E_{22}^{\mathrm{S}}\ I_{\mathrm{ex}}$ for RBM within ETB (STB [9]). Here red (blue) circles are semiconducting type I (II) nanotubes. (c) ((d)) is $E_{11}^{\mathrm{M}}\ I_{\mathrm{ex}}$ for RBM within ETB (STB [9]).

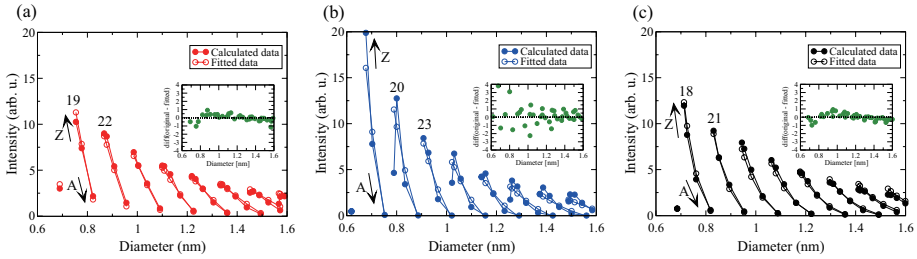

Figure 5: Calculated RBM intensity (solid symbols) of (a) semiconducting type I, (b) semiconducting type II, and (c) metallic nanotubes. Open symbols are fitted Raman intensity by Eq.(9). The label integers are the values of $(2n + m)$ = constant family, which are connect symbols by lines. Z (A) denotes (n, m) values near zigzag (armchair) nanotubes.

Table 1: The fitting parameters A, B, C, D, and E for Eq.(9). R^2 is a correlation coefficient of the fit.

	A	B	C	D	E	R^2
E_{22}^{SI}	1.588	-2.234	-3.199	13.849	-3.553	0.974
E_{22}^{SII}	1.562	-6.355	-2.998	15.744	-1.778	0.840
E_{11}^{M}	-0.116	0.919	0.434	3.694	1.560	0.980